Fabrication of the Funnel-Shaped Three-Dimensional Plasmonic Tip Arrays by Directional Photofluidization Lithography

Seungwoo Lee,[†,*] Jonghwa Shin,[‡] Yong-Hee Lee,[‡,§] and Jung-Ki Park[†,§,⊥,*]

[†]Department of Chemical and Biomolecular Engineering, [‡]Department of Physics, Graduate School of Nanoscience and Technology, [§]KAIST Institute for the Nanocentury, and [⊥]Graduate School of EEWS, Korea Advanced Institute of Science and Technology (KAIST), 335 Gwahangno, Yuseong-gu, Daejeon 305-701, Republic of Korea

ABSTRACT Plasmonics allow localization of an electromagnetic (EM) field into nanoscale "hotspots", a feature that is of technological significance due to potential applications related to spectroscopic sensing and nanofocusing. In relation to this, many researchers have sought to fabricate metallic nanostructures with sharp edges, as they provide much higher EM field enhancement compared with rounded structures. However, a fabrication method satisfying stringent requirements for the efficient EM field enhancement including three-dimensionality, vertical orientation, large-area fabrication, and tunability of structural features, which are of practical importance for efficient plasmonic light enhancement at hotspots, has yet to be achieved. Herein, we fabricate large-area, vertically aligned three-dimensional plasmonic tip (*i.e.*, nanofunnel) arrays with unprecedented flexibility in the control of the structural features by directional photofluidization lithography. Using this approach, the structural features of nanofunnel tips including the sharpness, shape, and orientation were precisely controlled in a scalable and deterministic manner. The effects of the structural features of the nanofunnel on the EM field enhancement were systematically investigated and analyzed, and the optimum tip features for maximum EM field enhancement were thereupon identified. The suggested nanofabrication technique and resulting structures will be of practical importance in spectroscopic and nanophotonic applications.

KEYWORDS: directional photofluidization lithography · plasmonic tips · azopolymer · nanofunnel · electromagnetic field enhancement

The plasmonic local enhancement of an electromagnetic (EM) field into nanoscale "hotspots" that exceeds the diffraction limit (or its wavelength scale) is of dramatic technological importance owing to their potential applications in surface-enhanced Raman scattering (SERS),[1−8] near-field imaging,[9,10] subwavelength scale laser,[11,12] and energy devices (solar cells).[13−16] One particular challenge in realizing EM field enhancement at hotspots is the ability to generate metallic nanostructures in a simple and reproducible manner. In particular, recent studies on the fabrication of plasmonic structures have focused on metallic nanostructures with sharp edges, since the EM fields near the sharp edges of metallic nanostructures are found to increase dramatically with increasing tip sharpness (or reducing the radius of curvature of metallic tips) (*i.e.*, due to an optical lightning rod effect).[17,18] To this end, various metallic nanostructures with sharp edges including nanoscale tips,[9,19−21] tapers,[22] trenches,[23] nanocrescent,[24] nanobowtie,[25] hole/disk,[26−28] and junctions with a gap[4,7] have been actually fabricated in efforts to address the challenges related to nanoscale enhancement of EM fields: a number of approaches for the fabrication of those metallic nanostructures have been proposed to date, including the metallization of readily prepared fiber tips,[9] complex multistep processes,[29] integration of metallic nanospheres,[3] electron beam lithography,[25] colloidal-templated metal deposition,[24] soft imprint lithography,[26−28] and controlled metal deposition and subsequent selective removing (*e.g.*, on-wire lithography).[4,7] However, fabrication methods that simultaneously meet stringent requirements such as three-dimensionality, vertical orientations, large-area fabrication with uniformity, and tunability of structural features, which are of practical importance for efficient plasmonic light enhancement at hotspots, have yet to be achieved.

Directional photofluidization lithography (DPL) makes it possible to generate diverse nanostructural motifs with precisely controlled sizes, shapes, and orientations in a very unique manner.[30] The success of DPL stems from the photoreconfiguration of pristine polymer arrays by means of directional photofluidization, a unique feature of azobenzene polymer (abbreviated as azopolymer).[30−35] In particular, in contrast with thermal-induced isotropic fluidization (or melting) of a thermoplastic polymer,[36,37]

*Address correspondence to ace51@kaist.ac.kr, jungpark@kaist.ac.kr.

Received for review July 23, 2010 and accepted October 29, 2010.

Published online November 22, 2010.
10.1021/nn1017507

© 2010 American Chemical Society

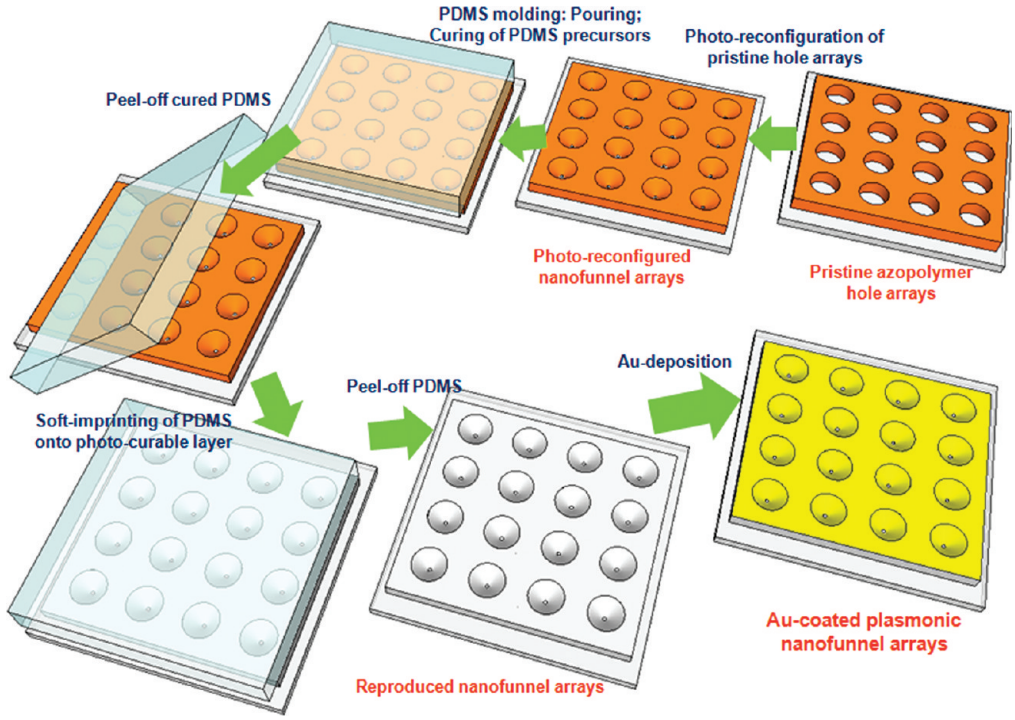

Figure 1. Schematic diagram of the working principle of directional photofluidic fabrication of plasmonic nanofunnel arrays (following the arrows from top right): radial photoreconfiguration of a pristine azopolymer hole array fabricated by micromolding in capillaries (MIMIC) using a solvent; molding transfer technique for the reproduction of the nanofunnel array onto photocurable materials; gold deposition onto the reproduced nanofunnel array.

photofluidization of azopolymer occurs only along the light polarization (directional photofluidization), and thus pristine arrays of azopolymer can be arbitrarily reconfigured in a parallel and scalable manner.[30−35] This impressive nature of azopolymer is produced by repeated photoisomerization of azobenzene molecules covalently attached to the polymeric main chain and their resulting anisotropic alignment in the direction perpendicular to the light polarization.[31] Importantly, greater flexibility in control over the structural features of the polymer array to be molded into metals or other materials makes it possible to fabricate unique structural motifs that would be very difficult to produce *via* other lithographic methods. For example, we reported that metallic nanostructures containing streamlined sharp edges or tips with nanoscale radius of curvature can be generated by DPL.[30] This unprecendented control over structural features enables the exploration of a variety of chemical and physical phenomena, such as surface plasmons, occurring in metallic nanostructures. Herein, by taking the advantages of DPL, we have sought to generate large-area, vertically aligned three-dimensional plasmonic tip arrays that are similar in appearance to a funnel; thus the name "nanofunnel". These procedures could provide unprecedented flexibility in the control of the structural features, including the sharpness, shape, and orientation of plasmonic tips. The effects of structural features of nanofunnel on nanoscale light enhancement were systematically investigated by experimental (*i.e.*, dark-field optical microscope, surface plasmonic extinction spectra, and Raman spectra) and theoretical (*i.e.*, finite-difference time-domain, FDTD) methods, and we thus identified the optimum tip diameter for maximum EM-field enhancement. We begin by describing the directional photofluidic fabrication procedures and then outlining the experimental and theoretical studies of the plasmonics. Finally, we examine the plasmonic EM field enhancement dependence on the geometry of nanofunnel tips.

RESULTS AND DISCUSSION

Fabrication of Gold-Coated Nanofunnel Arrays. The overall procedure for fabricating three-dimensional plasmonic nanofunnel arrays is summarized in Figure 1. Especially, we employed isotropic photofluidization of pristine azopolymer holes arranged in a tetragonal lattice. Micromolding in capillaries (MIMIC) with the use of a solvent was employed to fabricate pristine azopolymer hole arrays, as we previously reported;[30] polydisperse orange 3 was used as an azopolymer in this study.[30] The initial diameter and periodicity of the obtained pristine hole arrays (see Figure 2a) were 2 and 4 μm, respectively, and the thickness was 1.3 μm. The intensity and wavelength of the incident light were 23.0 mW/cm^2 and 488 nm, respectively. After photofluidization of the initial hole arrays, photoreconfigured nanofunnel arrays were reproduced by using a transfer molding technique: inversely replicated hard-polydimethylsiloxane (PDMS, ref 38) was soft-imprinted onto a photocurable material (NOA 65, Norland); photopolymerization and

the subsequent peel-off of hard-PDMS gave rise to the reproduced nanofunnel arrays with high fidelity (the contraction ratio was below 2%); gold was finally deposited onto the reproduced nanofunnel arrays by e-beam evaporation (the thickness of Au was controlled to be 20 nm).

The directional photofluidization, a key part of our proposed strategy, is the light-induced softening of solid azopolymer film at temperatures well below the glass transition temperature (T_g): recently, Karageorgiev *et al*. demonstrated that under light irradiation, the initial elastic solid of azopolymer thin film actually becomes a viscous fluid well below T_g, as evidenced from decreases in the slopes of load-penetration curves.[31] More importantly, this photosoftening of the azopolymer shows the polarization dependence in that the photofluidic movement occurs only in the direction parallel to the light polarization,[30,31] contrary to the previously reported thermal-induced liquefaction (SPEL) approaches,[36,37] where the thermally heated polymer exhibits isotropic flow. Understanding this directional photofluidization mechanism is a prerequisite for the broad subject of its practical application in nanofabrication. While this is being currently researched,[39] the resulting anisotropic alignment of azobenzene molecules after light irradiation likely gives rise to the anisotropic intermolecular interaction; thus anisotropic stress and consequent anisotropic photofluidization may occur in the polymer.[30,31] However, for a better understanding, the underlying mechanism of the directional photofluidization of azopolymers has to be further studied.

In this study, when circularly polarized light (right-handed circular polarization in this study) was irradiated for 6 min, the pristine cylindrical holes of azopolymer array were actually transformed into the inverted focal conic-shaped holes (nanofunnel) as a result of isotropic photofluidic movement (photofluidization) of the azopolymer (Figure 2a,b). Several interesting features observed with this photoreconfiguration of cylindrical holes into nanofunnel by using circularly polarized light are noteworthy: (i) Isotropic photofluidization was induced rather than anisotropic photofluidization by circularly polarized light irradiation. This is because linear polarization rotates clockwise, as the right-handed circularly polarized wave advances. Figure 3 panels a and b show the irradiation time evolution of photoreconfigured azopolymer hole arrays and their corresponding cross-sectional profiles measured by atomic force microscope (AFM). Indeed, the diameter of the initial holes (or tip diameter of nanofunnel) was isotropically reduced after radial photofluidization (see Figure 3a). Additionally, the modulation height of holes was spontaneously decreased with irradiation time (see Figure 3b), because the azopolymer moves toward vacancy areas (holes) during circularly polarized light irradiation. These observations clearly indicate that the photofluidic movement of the azopolymer took

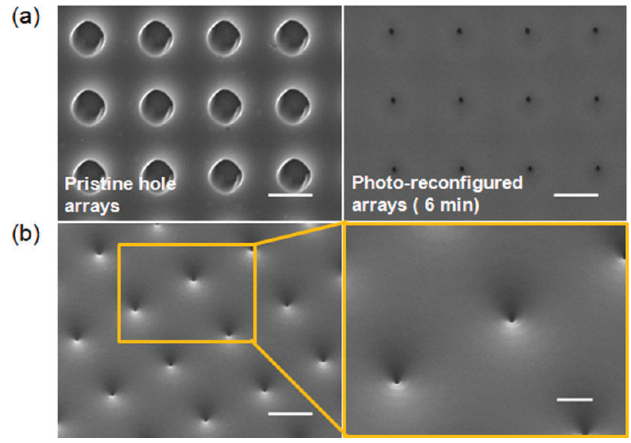

Figure 2. (a) SEM images of pristine hole array (left panel) and photoreconfigured nanofunnel array (6 min irradiated, right panel). (b) SEM images of azopolymer nanofunnel arrays taken at a tilted angle (40 degrees) (a close-up of nanofunnels marked by the yellow box, right panel).

place radially along the rotating linear polarization. (ii) The photofluidization caused the vertical walls of the pristine holes to become rounded, thus resulting in nanofunnel-shaped (or inverted focal conic-shaped) hole arrays as shown in Figure 2b (also see cross-sectional profile shown in Figure 3b). Additionally, the PDMS molds replicating the morphology of photoreconfigured azopolymer hole arrays clearly exhibited the focal conic-like morphology (Figure 3c), thus further supporting how the funnel is shaped. These obtained rounded walls after light irradiation can be attributed to interfacial energy minimization through a reduction of the surface area between air and polymer, as photofluidization might be also influenced by surface energy similar to thermal-induced smoothening of thermoplastic polymer.[36,37] Recently, we and Karageorgiev *et al*. reported that the rough edges or craves of pristine azopolymer films could be smoothed significantly by photofluidic surface energy minimization.[30,31] Our observations of this transition from vertical walls to rounded walls of azopolymer arrays further support that the azopolymer can become fluid under light irradiation. However, unfortunately, the theoretical mechanism for the fluidic motion of azopolymer under light irradiation has not yet been established completely. Therefore, we proposed qualitative explanation of the rounded wall on the basis of interfacial energy minimization to support experimental findings. (iii) When we used cylinder-shaped holes (punched holes in the azopolymer thin film) as pristine azopolymer arrays for the photofluidization process, three-dimensionally tapered focal cones or funnel can be oriented in the vertical direction with respect to the substrate. Therefore, efficient optical coupling by the normal irradiation of light, which is essential for high-quality nanofocusing or confocal Raman measurements,[40] should also be possible. (iv) The photofluidic reconfiguration of hole arrays ensures scalable and parallel processing; thus ho-

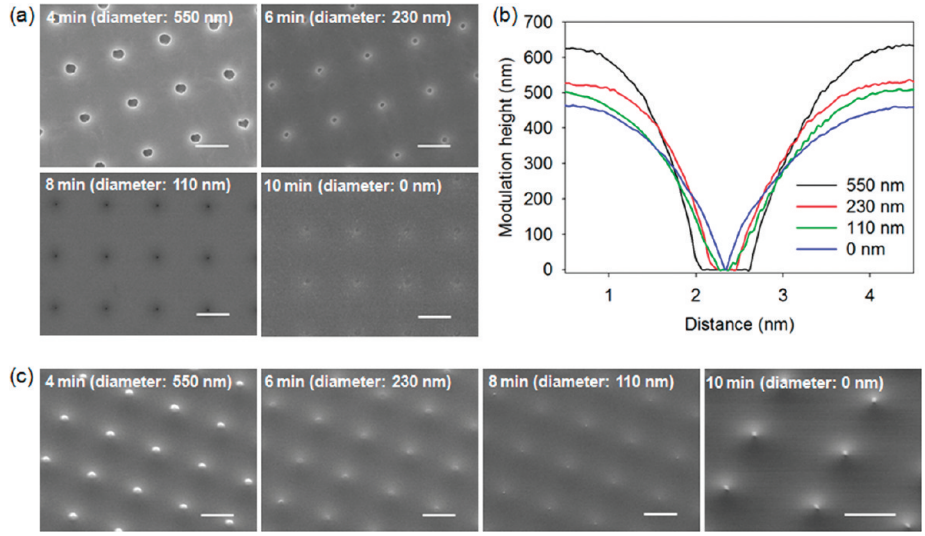

Figure 3. Irradiation time evolution of nanofunnel array with varying tip diameter. (a) SEM images of nanofunnel array with varying tip diameter. (b) Cross-sectional profile of nanofunnel measured by AFM. (c) SEM images of the PDMS molds replicating nanofunnel array with varying tip diameter. Scale bars are 2.5 μm (SEM image in panel c of 10 min, scale bar = 2.0 μm).

mogeneous EM field enhancement at a nanoscale, which is of technological significance for reproducible plasmonic enhanced spectroscopy (*e.g.*, SERS), can be achieved, in a simple and reliable manner. The excellent uniformity of photoreconfigured arrays over large areas is actually evidenced by the moiré fringe of the low-magnification SEM image (Supporting Information, Figure S1). (v) The diameter of tips of the nanofunnel can be precisely tuned between zero and several hundred nanometers merely by adjusting the irradiation time of circularly polarized light: a tip diameter of zero physically means that the radius of curvature of the tip was nearly zero. Indeed, decreases in the diameter of tips were observed with circularly polarized light irradiation, as shown in Figure 3a−c. This ability of precise control of the tip features allows one to study the effect of the tip sharpness on light enhancement in a systematic manner; the optimum tip diameter of nanofunnel for maximum EM field enhancement can be thus identified.

EM Field Enhancement near Plasmonic Nanofunnel Arrays. Figure 4a shows dark-field optical microscope (OM) images of 8 min irradiated nanofunnel arrays (having a tip diameter of around 110 nm) as a representative example: we illuminated the plasmonic nanofunnel arrays with unpolarized, spatially filtered, white light from a high-intensity fiber light source, and the scattered light was collected in the normal direction by using a microscopic objective lens (20×, Mitutoyo NIR M plan APO, numerical aperture (NA) = 0.42). To maximize the scattering from the obtained nanofunnel arrays, the source light was irradiated at a tilted angle (70°) with respect to the normal direction. The results presented in Figure 4a show that EM field-enhanced hotspots were clearly observed in the plasmonic nanofunnel arrays, whereas a flat gold surface prepared by deposition of gold (20 nm) onto a flat NOA layer exhibited an almost black image as will be shown later. Additionally, the observed hotspots were arranged in a tetragonal lattice corresponding to the configuration of the nanofunnel. Thus, we established that the EM field enhancements observed in Figure 4a occurred at the plasmonic nanofunnel. Some background hotspots in addition to the hotspots at the plasmonic nanofunnel were also partially observed; these are attributed to the Au roughness inherently caused by the e-beam evaporation process. Note that the ring shaped-EM field enhancement profiles were observed at the same regions, when the focal plane of the dark-field OM was located at around 500 nm height with respect to the end of tip (Figure 4b). This additional EM field enhancement resulted from constructive interference between the reflected and irradiated light. To rationalize the results of observed EM field enhancement in terms of the plasmonic electromagnetic mechanisms, we have calculated the electric field near the 20-nm thickness Au-coated nanofunnel arrays (8 min irradiated) using the finite-difference time-domain (FDTD) method with Yee's discretization scheme: details of the FDTD simulation are described in the Supporting Information, Figure S2.[41,42] Figure 4 panels c−e show the FDTD analysis results of the near-field profile at the surface of plasmonic nanofunnel. It is noteworthy that these calculated electric field distributions near the nanofunnel are in excellent agreement with the experimental measurements (dark-field OM images); from both the side-view (Figure 4c) and top-view with different heights (Figures 4d,e) of the near-field electric field profiles, it can be concluded that the bright spot distributions of dark-field OM images are responsible for the surface plasmon resonance (SPR) and resulting EM field enhancement near the tips.

Next, to demonstrate the effect of tip diameter on the EM field enhancement, we studied the dark-field

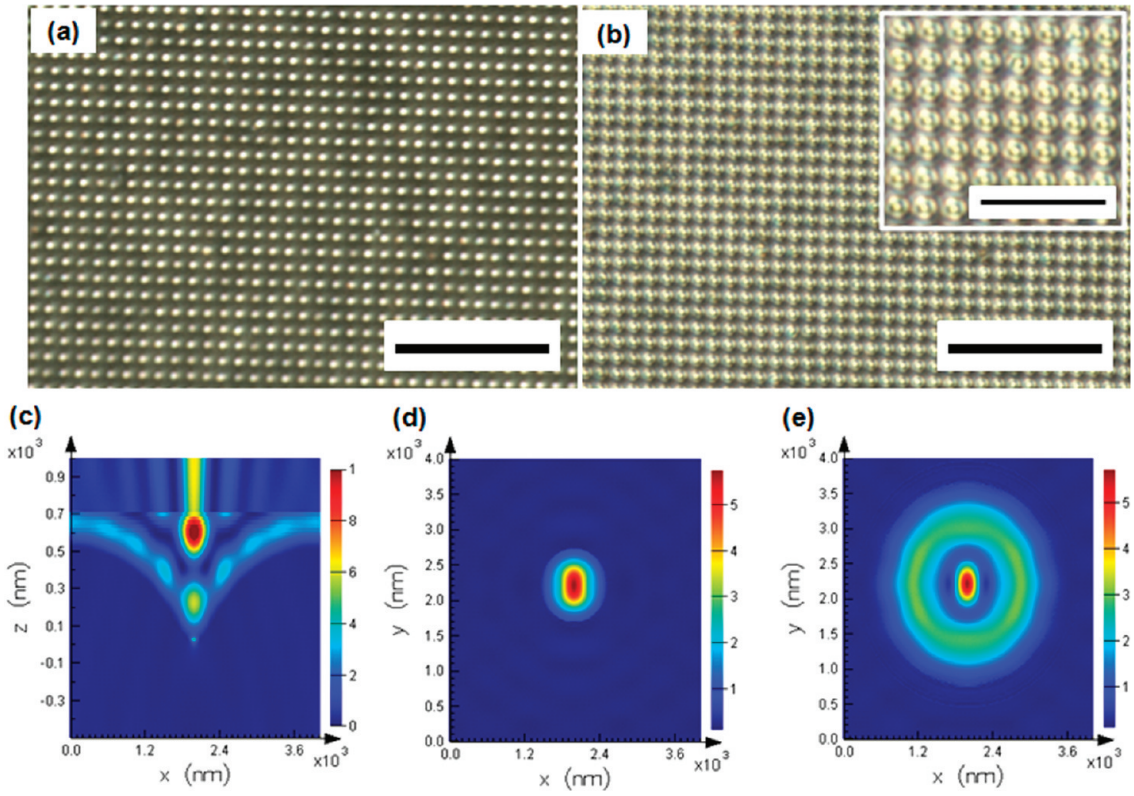

Figure 4. (a,b) Dark-field optical microscope (OM) images taken at different focal planes: at the tips (a); above the tips (b). Finite-difference time-domain (FDTD) simulation of the electric field enhancement at the surface of plasmonic nanofunnel (8 min irradiated, 110-nm diameter tip): (c) cross-sectional view of electric field enhancement profile; (d) top-view of the electric field enhancement profile taken at the tips; (e) top-view of the electric field enhancement profile taken above the tips. Scale bars are 40 μm (magnification dark-field OM, 16 μm).

OM images (Figure 5a) and corresponding extinction spectra (Figure 5b) of a series of Au-coated (20 nm thickness) nanofunnel arrays with varying tip diameters: dark-field OM images were taken at almost the same focal plane across the samples studied here; tip diameters ranging from zero to 550 nm were investigated, and the integration time was 20 s. The series of dark-field OM images and corresponding extinction spectra indicates that EM field extinctions gradually increased with decreasing tip diameters (in turn, increasing tip sharpness) due to a triggered optical lightning rod effect. Note, however, that, below 110 nm tip diameter (zero), a decrease in dark-field extinction was apparent even with decreasing tip diameter (Figure 5b). The electric-field enhancement in the results of the FDTD simulations approximately matched those of the measured spectra (Figure 5a,b), as shown in Figure 5c,d (0 and 110 nm tip diameter nanofunnel). This decrease in dark-field extinction at the sharpest tip is mainly due to intrinsic destructive interference at the tip apex, as reported previously: when linearly polarized light is irradiated, the destructive interference occurring at the tip apex leads to a reduction in the light focusing and concentration.[9] Furthermore, a lowered height of nanofunnel as a result of radial photofluidization may partially contribute to decreased dark-field extinction: during radial photofluidization, the flatness of the arrays increases due to the lowered height of nanofunnel as mentioned above; the amount of light that can be coupled with surface plasmons is spontaneously decreased. From the dark-field analysis results, it is concluded that the optimum tip diameter of plasmonic nanofunnel arrays for maximum EM field enhancement is 110 nm.

The prepared plasmonic nanofunnel arrays can be, of course, used for the measurements of SERS tunability. To do this, each array was adsorbed by methylene blue (MB) which is widely used as a SERS probe material, and the spectra were obtained by using a linearly polarized 632.8 nm, 50 μW diode laser (Melles Griot) implemented in a micro-Raman system (Ramboss, Dongwoo Optron Co., Ltd.). Specifically, the use of MB as a SERS probe material in our studies using a 632.8 nm laser can enhance the SERS signal due to the strong absorption band around 655 nm.[4] The dark-field OM image of MB adsorbed nanofunnel arrays is presented in Supporting Information, Figure S3. In particular, to clearly illustrate the issue of homogeneity of hotspots through a comparison, we also prepared an Au-coated (20-nm thickness) organized silica colloidal cluster (400-nm diameter, a) which is widely used as a SERS substrate (see the morphology shown in Figure 6a).[40−42] Whereas a colloidal cluster conventionally used as a SERS substrate was generally deposited by the thick metal (~200 nm)

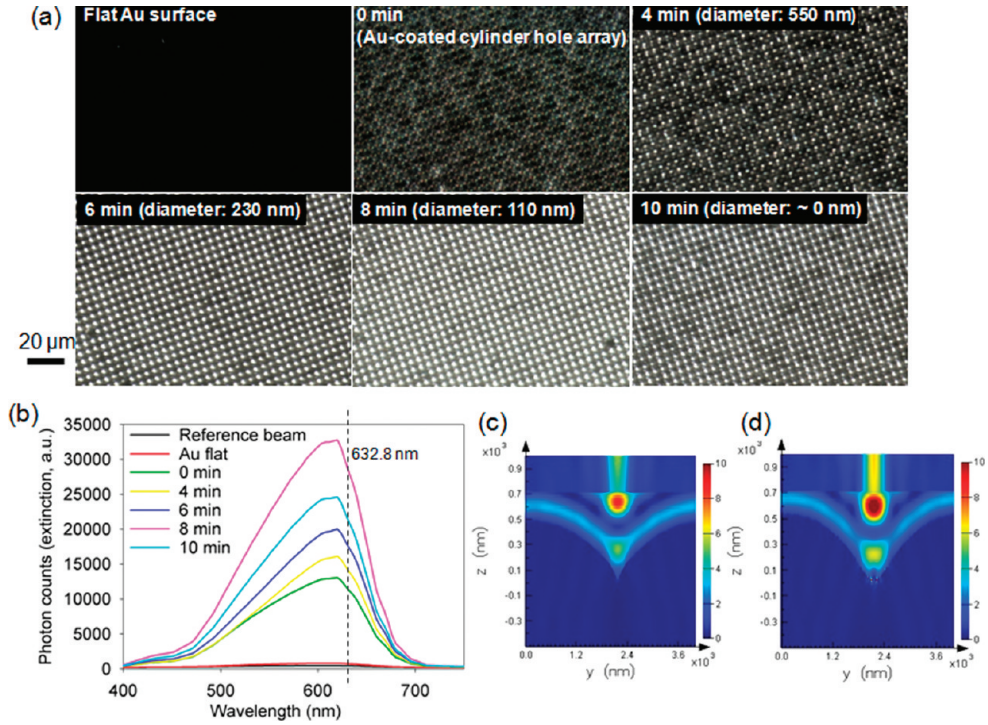

Figure 5. SPR mode characterization by using dark-field OM images and their extinction spectra: (a) a series of dark-field OM images for a flat Au surface (20-nm thickness), an Au-coated cylinder-shaped hole array (nonirradiated one), and plasmonic nanofunnel arrays with varying tip diameter. (b) Dark-field extinction spectra of corresponding dark-field OM images: the integration time was 20 s. FDTD simulation of the electric field enhancement associated with the resonance at 633 nm (cross-sectional view); (c) 0 nm diameter tip (8 min irradiated); (d) 110 nm diameter tip (10 min irradiated).

to increase the surface roughness and resulting EM field enhancement, we herein used a thin metal (20 nm) coated colloidal cluster to remove the roughness effect. This is because the goal of this study is to investigate the geometrical effect of a funnel-shaped plasmonic structure on the EM field enhancement. As shown in Figure 6b, the dark-field OM image of the Au-coated colloidal cluster shows that hotspots are heterogeneously distributed over the sample. Furthermore, the brightness of hotspots was found to be much lower than that of the plasmonic nanofunnel arrays (8 min irradiated, 110-nm tip diameter). Indeed, the dark-field extinction spectra corresponding to the dark-field OM image (Figure 6c) showed much lower SPR resonance compared with the plasmonic nanofunnel arrays (see Figure 4a, 8 min irradiated, 110-nm tip diameter): the integration time was 20 s. Accordingly, confocal Raman microscope images (Figure 7a) clearly indicated that the plasmonic nanofunnel arrays (110-nm tip diameter, 8 min irradiated) showed homogeneous, well-ordered, and much brighter hotspots, whereas the hotspots from the Au-coated colloidal cluster were heterogeneously distributed together with much lower brightness. Figure 7b shows the measured Raman spectra of MB from a series of prepared nanofunnel arrays with varying tip diameter: for a careful analysis of the SERS signals on the tip diameter, the intense mode of MB vibration at 1628 cm^{-1} was investigated for comparison. As shown in Figure 7b, the obtained signals for plasmonic nanofunnel arrays were found to be increased with the dark-field extinction: the broad and intense SPR modes of nanofunnel arrays, as evidenced by the results of dark-field extinction spectra, were in resonance with 632.8 nm (see Figure 5b). A 110-nm-tip di-

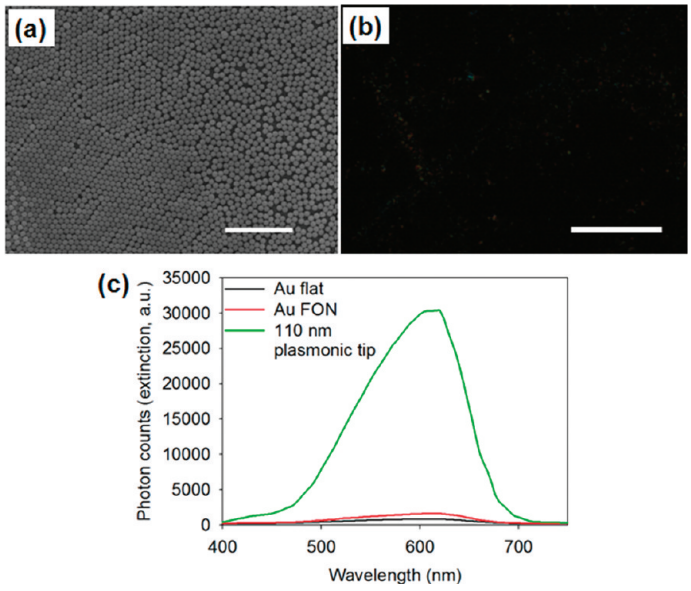

Figure 6. (a) SEM image of the obtained organized silica colloidal cluster after Au-deposition with 20-nm thickness (Au film over nanosphere, Au FON); (b) dark-field OM image corresponding to the SEM image in Supporting Information, Figure S9; (c) dark-field extinction spectra: Au-coated flat surface (black line); Au-coated colloidal cluster (Au FON, red line); plasmonic nanofunnel array (green line). Scale bars are (a) 5 and (b) 40 μm.

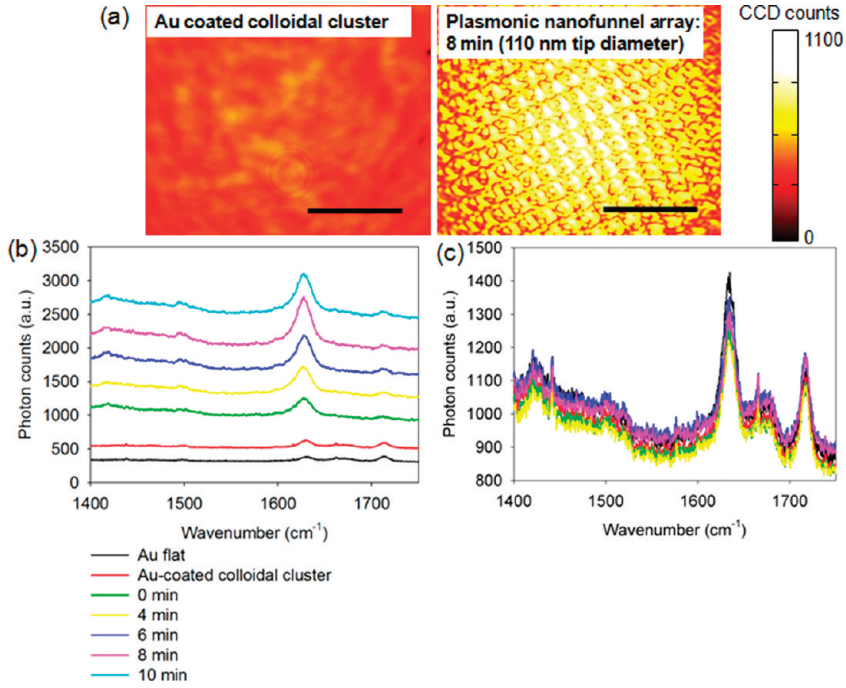

Figure 7. Confocal Raman microscopic analysis of plasmonic nanofunnel arrays: (a) confocal Raman microscope images of an Au-coated colloidal cluster (20-nm thickness, left panel) and plasmonic nanofunnel arrays with 110-nm tip diameter (right panel); (b) MB Raman spectra of an Au-coated flat surface, an Au-coated colloidal cluster, and plasmonic nanofunnel arrays with varying tip diameter; (c) uniform Raman spectra from a plasmonic nanofunnel array with 110-nm tip diameter: variations in the SERS signals obtained from six different positions in an area of 1 cm^2 was less than 14%. Scale bars are 20 μm.

ameter plasmonic nanofunnel array yielded the largest SERS response, 12 times higher than that of Au-flat film: using a previously reported protocol,[40] the enhancement factor at the 110-nm diameter tip of the plasmonic nanofunnel (intense band at 1628 cm^{-1}) was calculated to be around 10^8-10^9. To quantitatively examine the homogeneity over large-area plasmonic nanofunnel arrays in greater detail, we also checked SERS spectra from six different positions in an area of 1 cm^2 (a 110-nm diameter tip was used as a representative example). As can be seen from the SERS spectra from the six different positions (Figure 7c), the fabricated plasmonic nanofunnel arrays showed excellent uniformity and reproducibility of the SERS signals over a large area: the variation was less than 14%.

Control of the Shapes of Nanofunnel Tip. In addition to tunability of dimensions, we could precisely control the shapes of the nanofunnel tip, by using anisotropic photofluidization instead of isotropic photofluidization. By way of demonstration, we employed right-handed elliptically polarized light with an identical light intensity: the ellipticity, defined as the ratio of the minor axis to the major axis, was 0.18 (see the schematic illustration of Figure 8a); the irradiation time was 12 min. According to our previous report, the degree of directional photofluidization is also strongly influenced by the intensity of light as well as the irradiation time.[30] Therefore, the irradiation of elliptically polarized light could lead to photoreconfiguration of pristine holes into line-shaped tips as a result of anisotropic photofluidization: in the direction of the major axis of elliptical polarization, photofluidization was facilitated much more efficiently compared with that in the direction of the minor axis, resulting in anisotropically photoreconfigured line-shaped tips rather than circular tips, as shown in the right panel of Figure 8a. The length in the long axis was 1 μm. Furthermore, the use of elliptically polarized light endows the photofluidic fabrication process with additional controllability over the structural orientation as well as shapes. For example, when the major axis of elliptical polarization is tilted with respect to the original lattice (tetragonal in this study) (see the schematic illustration of Figure 8b), the structures of the obtained photoreconfigured arrays also can be oriented according to the tilting angle of elliptically polarized light: the tilt angle of elliptical polarization and irradiation time were 45° and 12 min, respectively. In fact, we obtained plasmonic nanofunnel arrays with a line-shaped anisotropic tip and 45 °C orientation with respect to the tetragonal lattice, as presented in the right panel of Figure 8b: the ratio of long axis to short axis was 0.2 (the length of line was 1 μm), and the gap between adjunct walls was zero. This anisotropically defined tip exhibits polarization dependence on the SERS signal sensitivity (see Figure 8c). In particular, the SERS signal excited by perpedicular polarization to the long axis of the line-shaped tip was maximized, whereas the parallel polarization showed minimized SERS signal excitation: the perpendicular polarization showed 4 times larger excitation than the parallel polarization. In the anisotropic plasmonic structures, when a parallel polarized light with respect to the major axis of structure

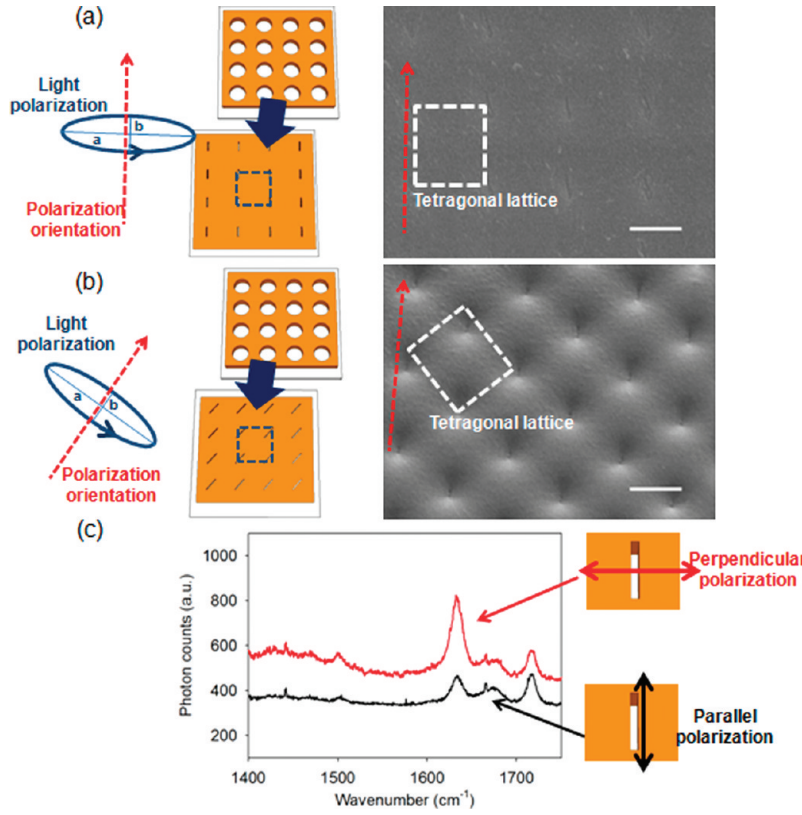

Figure 8. Anisotropic photofluidic reconfiguration of pristine azopolymer hole arrays: (a) schematic illustration (left panel) of anisotropic photoreconfiguration by using elliptically polarized light with parallel orientation with respect to the structural lattice (tetragonal) and the SEM image of resulting plasmonic nanofunnel arrays with an anisotropic shape (line) of the tip; (b) schematic illustration (left panel) of the anisotropic photoreconfiguration by using elliptically polarized light with a 45° tilted orientation with respect to the structural lattice (tetragonal) and a SEM image of the resulting plasmonic nanofunnel arrays with an anisotropic shape (line) of the tip and 45 deg tilted structural orientation; (c) polarization dependence of MB Raman spectra for plasmonic nanofunnel arrays with line-shaped tips (Figure 8a). Scale bars are 2.5 μm.

was irradiated, the hotspots to be excited almost disappeared, resulting in polarization-selective SERS signal sensitivity, as described above.[40,45] Therefore, directional photofluidic fabrication provides unprecedented control of the plasmonic structures and their optical properties.

CONCLUSION

We have prepared plasmonic nanofunnel arrays with tunable tips by means of directional photofluidization and analyzed EM field enhancement by experimental and theoretical methods. The experimental observations and related conclusions presented above are fundamentally and technologically important for the following reasons. First, directional photofluidization allows the realization of plasmonic sharp edge structures with a very high flexibility in the control of structural features such as tip sharpness, shapes, and orientations. This unique ability of directional photofluidization enables the fabrication of metallic tip structures with tunable plasmonic properties in a scalable and parallel manner. Second, precise control of the tip sharpness *via* directional photofluidization provides important insights concerning the optimum tip diameter associated with these types of plasmonic nanostructures. From systematic studies enabled by this fabrication approach, we found that the least sharp tip, a 110-nm diameter tip in this study, can maximize the EM field enhancement and also the SERS signal. In general, at a metal-covered tip apex, the intrinsic destructive interference of surface plasmons, when linearly polarized light is irradiated, leads to a reduction in the light focusing and concentration. To address this problem of EM field degradation at the tip region, irradiation *via* the radially polarization propagating mode (also called the radial doughnut mode) has been proposed to allow surface plasmons to interfere constructively at the tip apex.[9] From our observations, we also can now consider strategies for EM field enhancement within sharp-edge structures with the vertically aligned nanofunnel having controlled tip sharpness as well as by adjusting the light polarization. Finally, it has been demonstrated that the DPL process provides a relatively simple and reliable method to fabricate large-area metallic nanostructures with sharp edges for reproducible EM field enhancement.

However the directional photofluidic fabrication of plasmonic structures described in this paper has limitations. While the plasmonic nanofunnel can give rise to efficient EM field enhancement, most of the area is not effective and consequently wasted space. This is because the fill factor of arrays is relatively

low (~50%): the periodicity of the pattern is 4 μm. In this study, as a proof of concept, we used the large-spaced PDMS (~4 μm) post arrays to fabricate the large-area pristine azopolymer arrays by using the MIMIC method, because the penetration of the polymer solution can be triggered as the dimension of microfluidic channel increases.[46] It is, however, possible to generate highly dense pristine azopolymer arrays, in the same way that nanoimprint lithography and block copolymer lithography enables the high density polymer patterning. This work is now underway, and the details will be reported in a forthcoming paper. We believe that the unique ability of this nanofabrication approach and the obtained structures are expected to be of significant utility in spectroscopy and nanophotonics.

METHODS

Preparation of PDMS Molds. The master of hole arrays was fabricated by conventional photolithography. The height and diameter of the fabricated circular hole arrays were 1.8 and 2 μm, respectively. The periodicity was 4 μm. To obtain the PDMS mold, a PDMS prepolymer and an initiator (Sylgard 184, Dow Corning, Midland, MI) were mixed at a 7:1 ratio (by weight), and subsequently degassed by vacuum suction. The degassed solution of PDMS was then poured against a prepared master carefully to prevent the generation of bubbles. Finally, the PDMS solution was cured at 70 °C in an oven for 30 min. After it was completely cured, the PDMS mold was released from the master. Supporting Information, Figure S4 displays the obtained PDMS mold: the structural features of the PDMS mold including the height, width, and periodicity were comparable to those of the master.

Micromolding in Capillaries (MIMIC) with Solvent. Details of the MIMIC process are as follows (also see Supporting Information, Figure S5): The glass substrates used here were cleaned by sonication in acetone, ethanol, and deionized water. After drying, the PDMS mold was placed onto a cleaned glass substrate to form the microcapillaries. The azopolymer solution (in NMP, 10 wt %) was then dropped into the entrance of the microcapillaries. Once the capillaries were filled with the azopolymer solution, the solvent was completely evaporated at 40 °C for 1 day. Finally, the PDMS mold was peeled-off from the substrate. Azopolymer circular hole arrays replicating the molds were thus obtained.

Preparation of Au-Coated Organized Silica Colloidal Clusters. Monodisperse silica colloidal particles of 400-nm diameter were synthesized using the Stöber method.[47] After rinsing, the obtained silica powders were dispersed in ethanol (30 vol %). The resulting silica colloidal suspension was dropped onto a precleaned silicon wafer and then spin-coated (1770 rpm, 30 s). Au with 20-nm thickness was deposited onto silica colloidal clusters by e-beam evaporation.

Characterization of Photofluidization. The structures of the azopolymer arrays were investigated by means of scanning electron microscopy (SEM, FEI, Sirion), atomic force microscopy (AFM, PSIA XEI-100 systems), and optical microscopy measurements in transmission mode (OM, Olympus, BX51).

Optical Setup for Light Irradiation. The optical set up for light irradiation process is described in Supporting Information, Figure S6. The intensity and polarization of the beams were controlled using a neutral density (ND) filter and a wave plate, respectively. The initial Gaussian laser beam was homogenized by using a spatial filter, while its intensity and polarization were precisely controlled by neutral density filter and wave plate, respectively. The irradiation time was precisely controlled by using an electronic shutter.

Transfer Molding Technique. Photoreconfigured nanofunnel arrays were reproduced by using a transfer molding technique: inversely replicated hard-polydimethylsiloxane (PDMS, ref 38) was soft-imprinted onto a photocurable material (NOA 65, Norland); photopolymerization by UV irradiation (300 mW/cm^2, 10 min) and the subsequent peel-off of hard-PDMS gave rise to the reproduced nanofunnel arrays.

Measurement of Dark-Field OM Images and Extinction Spectra. The microreflectance system was built on a standard optical microscope (OM, Olympus, BX51): a thermo-electrically cooled CCD detector (DV401A-BC, iDUS CCD detector, Andor technology) was equipped. An unpolarized, spatially filtered 100 W halogen light source (Fiber Illuminator OSL1) was irradiated at an incident angle of 70° (dark-field illumination). The scattered light was collected by a 20× microscopic objective lens (Mitutoyo NIR M plan APO, numerical aperture (NA) = 0.42) and analyzed by the spectrometer. The schematic illustration of optical setup is described in Supporting Information, Figure S7.

Measurement of Raman Spectra. The spectra were obtained by using a linearly polarized 632.8 nm, 50 μW diode laser (Melles Griot) implemented in a home-built micro-Raman system (Ramboss, Dongwoo Optron Co., Ltd.) equipped with a thermo-electrically cooled CCD detector: focused beam diameter was 1 μm; the integration time was 3 min. The schematic illustration of experimental setup for Raman analysis is described in Supporting Information, Figure S8.

Acknowledgment. This publication was based on research supported by a grant (Code No. 09K1501-02510) from the "Center for Nanostructured Materials Technology" under the "21st Century Frontier R&D Programs" of the Ministry of Education, Science, and Technology of Korea. The authors also appreciate partial support from the Brain Korea 21 Program and WCU program (EEWS) at KAIST. S.L. acknowledges support from the Korea Science and Engineering Foundation (Code No. S2-2008-000-01855-1). S. L. would also like to thank Dongwoo Optron Co., Ltd., for the establishment of a home-built micro-Raman system (Ramboss system).

Supporting Information Available: Low magnification SEM image of photoreconfigured polymer arrays (Figure S1); a description of FDTD simulation, 3D AFM images based on the weighted-average revolution (Figure S2); dark-field optical microscopic image of methylene blue adsorbed onto plasmonic nanofunnel arrays (Figure S3); a description of SERS enhancement factor calculation; SEM image of PDMS mold used for MIMIC (Figure S4); schematic illustration of MIMIC process (Figure S5); schematic illustration of optical setup for light irradiation (Figure S6); the experimental geometry of dark-field optical microscopic measurement (Figures S7, S9); the experimental geometry of Raman setup (Figure S8, S9). This material is available free of charge *via* the Internet at http://pubs.acs.org.

REFERENCES AND NOTES

1. Stöckle, R. M.; Suh, Y. D.; Deckert, V.; Zenobi, R. Nanoscale Chemical Analysis by Tip-Enhanced Raman Spectroscopy. *Chem. Phys. Lett.* **2000**, *318*, 131–136.
2. Gunnarsson, L.; Bjerneld, E. J.; Petronis, S.; Kasemo, B.; Käll, M. Interparticle Coupling Effects in Nanofabricated Substrates for Surface-Enhanced Raman Scattering. *Appl. Phys. Lett.* **2001**, *78*, 802–804.
3. Wang, H.; Levin, C. S.; Halas, N. J. Nanosphere Arrays with Controlled Sub-10-nm Gaps as Surface-Enhanced Raman Spectroscopy Substrates. *J. Am. Chem. Soc.* **2005**, *127*, 14992–14993.
4. Qin, L.; Zou, S.; Xue, C.; Atkinson, A.; Schatz, G. C.; Mirkin, C. A. Designing, Fabricating, and Imaging Raman Hot Spots. *Proc. Natl. Acad. Sci. U.S.A.* **2006**, *103*, 13300–13303.
5. Ward, D. R.; Grady, N. K.; Levin, C. S.; Halas, N. J.; Wu, Y.; Nordlander, P.; Natelson, D. Electromigrated Nanoscale Gaps for Surface-Enhanced Raman Spectroscopy. *Nano Lett.* **2007**, *7*, 1396–1400.
6. Chen, C.; Hutchison, J. A.; Clemente, F.; Kox, R.; Uji-I, H.; Hofkens, J.; Lagae, L.; Maes, G.; Borghs, G.; van Dorpe, P. Direct Evidence of High Spatial Localization of Hot Spots in Surface-Enhanced Raman Scattering. *Angew. Chem., Int. Ed.* **2009**, *48*, 9932–9935.
7. Wei, W.; Li, S.; Millstone, J. E.; Banholzer, M. J.; Chen, X.; Xu,

X.; Schatz, G. C.; Mirkin, C. A. Surprisingly Long-Range Surface-Enhanced Raman Scattering (SERS) on Au−Ni Multisegmented Nanowires. *Angew. Chem., Int. Ed.* **2009**, *48*, 4210–4212.
8. Li, J. F.; Huang, Y. F.; Ding, Y.; Yang, Z. L.; Li, S. B.; Zhou, X. S.; Fan, F. R.; Zhang, W.; Zhou, Z. Y.; Wu, D. Y.; Ren, B.; Wang, Z. L.; Tian, Z. Q. Shell-Isolated Nanoparticle-Enhanced Raman Spectroscopy. *Nature* **2010**, *464*, 392–395.
9. Bouhelier, A.; Renger, J.; Beversluis, M. R.; Novotny, L. Plasmon-Coupled Tip-Enhanced Near-Field Optical Microscopy. *J. Microsc.* **2003**, *210*, 220–224.
10. Kawata, S.; Inouye, Y.; Verma, P. Plasmonics for Near-Field Nano-Imaging and Superlensing. *Nat. Photon.* **2009**, *3*, 388–394.
11. Oulton, R. F.; Sorger, V. J.; Zentgraf, T.; Ma, R.-M.; Gladden, C.; Dai, L.; Bartal, G.; Zhang, X. Plasmon Lasers at Deep Subwavelength Scale. *Nature* **2009**, *461*, 629–632.
12. Noginov, M. A.; Zhu, G.; Belgrave, A. M.; Bakker, R.; Shalaev, V. M.; Narimanov, E. E.; Stout, S.; Herz, E.; Suteewong, T.; Wiesner, U. Demonstration of a Spaser-Based Nanolaser. *Nature* **2009**, *460*, 1110–1112.
13. Catchpole, K. R.; Polman, A. Plasmonic Solar Cells. *Opt. Express* **2008**, *16*, 21793–21800.
14. Pala, R. A.; White, J.; Barnard, E.; Liu, J.; Brongersma, M. L. Design of Plasmonic Thin-Film Solar Cells with Broadband Absorption Enhancements. *Adv. Mater.* **2009**, *21*, 3504–3509.
15. Atwater, H. A.; Polman, A. Plasmonics for Improved Photovoltaic Devices. *Nat. Mater.* **2010**, *9*, 205–213.
16. Min, C.; Li, J.; Veronis, G.; Lee, J.-Y.; Fan, S.; Peumans, P. Enhancement of Optical Absorption in Thin-Film Organic Solar Cells through the Excitation of Plasmonic Modes in Metallic Gratings. *Appl. Phys. Lett.* **2010**, *96*, 133302/1–3.
17. Novotny, L.; Bian, R. X.; Xie, X. S. Theory of Nanometric Optical Tweezers. *Phys. Rev. Lett.* **1997**, *79*, 645–648.
18. Kelly, K. L.; Coronado, E.; Zhao, L. L.; Schatz, G. C. The Optical Properties of Metal Nanoparticles: The Influence of Size, Shape, and Dielectric Environment. *J. Phys. Chem.* **2003**, *107*, 668–677.
19. Stockman, M. Nanofocusing of Optical Energy in Tapered Plasmonic Waveguides. *Phys. Rev. Lett.* **2004**, *93*, 137404/1−4.
20. Ropers, C.; Neacsu, C.; Elsaesser, T.; Albrecht, M.; Raschke, M.; Lienau, C. Grating-Coupling of Surface Plasmons onto Metallic Tips: A Nanoconfined Light Source. *Nano Lett.* **2007**, *7*, 2784–2788.
21. Lindquist, N. C.; Nagpal, P.; Lesuffleur, A.; Norris, D. J.; Oh, S.-H. Three-Dimensional Plasmonic Nanofocusing. *Nano Lett.* **2010**, *10*, 1369–1373.
22. Søndergaard, T.; Bozhevolnyi, S. I.; Beermann, J.; Novikov, S. M.; Devaux, E.; Ebbesen, T. W. Resonant Plasmon Nanofocusing by Closed Tapered Gaps. *Nano Lett.* **2010**, *10*, 291–295.
23. Volkov, V. S.; Bozhevolnyi, S. I.; Rodrigo, S. G.; Martín-Moreno, L.; García-Vidal, F. J.; Devaux, E.; Ebbesen, T. W. Nanofocusing with Channel Plasmon Polaritons. *Nano Lett.* **2009**, *9*, 1278–1282.
24. Wu, L. Y.; Ross, B. M.; Lee, L. P. Optical Properties of the Crescent-Shaped Nanohole Antenna. *Nano Lett.* **2009**, *9*, 1956–1961.
25. Sundaramurthy, A.; James Schuck, P.; Conley, N. R.; Fromm, D. P.; Kino, G. S.; Moerner, W. E. Toward Nanometer-Scale Optical Photolithography: Utilizing the Near-Field of Bowtie Optical Nanoantenna. *Nano Lett.* **2006**, *6*, 355–360.
26. Stewart, M. E.; Mack, N. H.; Malyarchuk, V.; Soares, J. A. N. T.; Lee, T.-W.; Gray, S. K.; Nuzzo, R. G.; Rogers, J. A. Quantitative Multispectral Biosensing and 1D Imaging Using Quasi-3D Plasmonic Crystals. *Proc. Natl. Acad. Sci. U.S.A.* **2006**, *103*, 17143–17148.
27. Yao, J.; Stewart, M. E.; Maria, J.; Lee, T.-W.; Gray, S. K.; Rogers, J. A.; Nuzzo, R. G. Seeing Molecules by Eye: Surface Plasmon Resonance Imaging at Visible Wavelengths with High Spatial Resolution and Submonolayer Sensitivity. *Angew. Chem., Int. Ed.* **2008**, *47*, 5013–5017.
28. Baca, A. J.; Truong, T. T.; Cambrea, L. R.; Montgomery, J. M.; Gray, S. K.; Abdula, D.; Banks, T. R.; Yao, J.; Nuzzo, R. G.; Rogers, J. A. Molded Plasmonic Crystals for Detecting and Spatially Imaging Surface Bound Species by Surface-Enhanced Raman Scattering. *Appl. Phys. Lett.* **2009**, *94*, 243109/1–3.
29. Vedantam, S.; Lee, H.; Tang, J.; Conway, J.; Staffaroni, M.; Yablonovitch, E. A Plasmonic Dimple Lens for Nanoscale Focusing of Light. *Nano Lett.* **2009**, *9*, 3447–3452.
30. Lee, S.; Shin, J.; Lee, Y.-H.; Fan, S.; Park, J.-K. Directional Photofluidization Lithography for Nanoarchitectures with Controlled Shapes and Sizes. *Nano Lett.* **2010**, *10*, 296–304.
31. Karageorgiev, P.; Neher, D.; Schulz, B.; Stiller, B.; Pietsch, U.; Giersig, M.; Brehmer, L. From Anisotropic Photofluidity towards Nanomanipulation in the Optical Near-Field. *Nat. Mater.* **2005**, *4*, 699–703.
32. Li, Y.; He, Y.; Tong, X.; Wang, X. Photoinduced Deformation of Amphiphilic Azo Polymer Colloidal Spheres. *J. Am. Chem. Soc.* **2005**, *127*, 699–700.
33. Li, Y.; Tong, X.; He, Y.; Wang, X. Formation of Ordered Mesoporous Films from *in Situ* Structure Inversion of Azo Polymer Colloidal Arrays. *J. Am. Chem. Soc.* **2006**, *128*, 2220–2221.
34. Liu, J.; He, Y.; Wang, X. Azo Polymer Colloidal Spheres Containing Different Amounts of Functional Groups and Their Photoinduced Deformation Behavior. *Langmuir* **2008**, *24*, 678–682.
35. Liu, J.; He, Y.; Wang, X. Size-Dependent Light-Driven Effect Observed for Azo Polymer Colloidal Spheres with Different Average Diameters. *Langmuir* **2009**, *25*, 5974–5979.
36. Chou, S. Y.; Xia, Q. Improved Nanofabrication through Guided Transient Liquefaction. *Nat. Nanotechnol.* **2008**, *3*, 295–300.
37. Wang, Y.; Liang, X.; Liang, Y.; Chou, S. Y. Sub-10-nm Wide Trench, Line, and Hole Fabrication Using Pressed Self-Perfection. *Nano Lett.* **2008**, *8*, 1986–1990.
38. Lin, R.; Rogers, J. A. Molecular-Scale Soft Imprint Lithography for Alignment Layers in Liquid Crystal Devices. *Nano Lett.* **2007**, *7*, 1613–1621.
39. Juan, M. L.; Plain, J.; Bachelot, R.; Royer, P.; Gray, S. K.; Wiederrecht, G. P. Multiscale Model for Photoinduced Molecular Motion in Azo Polymers. *ACS Nano* **2009**, *3*, 1573–1579.
40. Im, H.; Bantz, K. C.; Lindquist, N. C.; Haynes, C. L.; Oh, S.-H. Vertically Oriented Sub-10-nm Plasmonic Nanogap. *Nano Lett.* **2010**, *10*, 2231–2236.
41. Dick, L. A.; McFarland, A. D.; Haynes, C. L.; Van Duyne, R. P. Metal Film over Nanosphere (MFON) Electrodes for Surface-Enhanced Raman Spectroscopy (SERS): Improvements in Surface Nanostructure Stability and Suppression of Irreversible Loss. *J. Phys. Chem. B* **2002**, *106*, 853–860.
42. Stuart, D. A.; Yonzon, C. R.; Zhang, X.; Lyandres, O.; Shah, N. C.; Glucksberg, M. R.; Walsh, J. T.; Van Duyne, R. P. Glucose Sensing Using Near-Infrared Surface-Enhanced Raman Spectroscopy: Gold Surfaces, 10-Day Stability, and Improved Acccuracy. *Anal. Chem.* **2005**, *77*, 4013–4019.
43. Fan, S.; Villeneuve, P. R.; Joannopoulos, J. D. Large Omnidirectional Band Gaps in Metallodielectric Photonic Crystals. *Phys. Rev. B* **1996**, *54*, 11245–111251.
44. Yee, K. S. Numerical Solution of Initial Boundary Value Problems Involving Maxwell's Equations in Isotropic Media. *IEEE Trans. Antennas Propag.* **1996**, *AP-14*, 302–307.
45. Yoon, I.; Kang, T.; Choi, W.; Kim, J.; Yoo, Y.; Joo, S.-W.; Park, Q.-H.; Ihee, H.; Kim, B. Single-Nanowire-on-Film as an Efficient SERS-Active Platform. *J. Am. Chem. Soc.* **2009**, *131*, 758–762.
46. Kim, E.; Whitesides, G. M. Imbibition and Flow of Wetting Liquids in Noncircular Capillaries. *J. Phys. Chem. B* **1997**, *101*, 855–863.
47. Stöber, W. Controlled Growth of Monodisperse Silica Spheres in the Micron Size Range. *J. Colloid Interface Sci.* **1968**, *26*, 62–69.